EUROPEAN COMMISSION
DIRECTORATE-GENERAL
Joint Research Centre

Institute for the Protection and Security of the Citizen

Experimental analysis of the shear transfer mechanism in a composite bridge beam manufactured from advanced polymer composites.

E. Gutiérrez, S. Primi
European Laboratory for Structural Assessment (ELSA)
I-21020 Ispra (VA), Italy

Institute for the Protection and Security of the Citizen

2005

EUR 21549 EN

European Commission
Directorate-General Joint Research Centre
Institute for the Protection and Security of the Citizen

Contact information
Address:ELSA TP 480
E-mail: eugenio.gutierrez@jrc.it
Tel.: ++-39-0332-785711
Fax: ++39-0332-789049

http://www.elsa.jrc.it
http://www.jrc.cec.eu.int

EU 21549 EN
Luxembourg: Office for Official Publications of the European Communities

Printed in Italy

The mission of the Joint Research Centre is to provide customer-driven scientific and technical support for the conception, development, implementation and monitoring of European Union policies. As a service of the European Commission, the JRC functions as a reference centre of science and technology for the Union. Close to the policy-making process, it serves the common interest of the Member States, while being independent of special interests, whether private or national.

1 Introduction

In this report we examine the structural interaction between advanced composite materials and reinforced concrete when combined to construct so-called, *composite-action* structural elements. The more usual meaning of composite ―outside the civil engineering field― refers to an important class of engineering materials predominantly used in mechanical and aeronautical applications. Composite materials are those consisting of two or more parts, and, although in theory many materials conform to this broad definition, it is only when significant changes occur as a result of the combination of macroscopically differing phases that the term composite is used.

According to this definition, reinforced concrete (RC) is a composite material, however, as it is a composite used exclusively in civil engineering, it is not generally included in the composite materials corpus. Civil engineers design structures using RC but they do not resort to composite material design procedures when doing so, in fact, the term composite in civil engineering is not used in this context at all. Until recently *composite-action beams* in civil engineering applied to cast-in-place concrete slabs connected to supporting steel beams; but now that the use of Fibre Reinforced Polymer composites (FRP) is progressively gaining ground in the field of civil engineering, the liberal use of the word composite may lead to confusion as to whether one is referring to a composite-action structure or one where composite FRP materials are used as part of the load bearing elements. If we now consider a composite-action structure, such as a bridge, whose main load carrying beams are manufactured with FRP materials rather than steel, then we could define such structures as doubly composite (C^2). The PUMACOM project {3} is such an example, whose aim was to develop a new-build composite-action bridge assembled using advanced composite carbon fibre beams, shear-locked onto a standard reinforced concrete deck.

In this report we examine in detail the performance of a key component of any composite-action beam: the transfer of shear loads from the main support beam to the RC slab. We consider only the experimental behaviour of a full-scale bridge beam subassembly, with a view to identifying the gross mechanical properties of such a system. Our scope is to understand and qualify thestrain distributions at the interface between the RC deck and the carbon fibre composite beam used as the main structural elelement, hoping to provide experimental data set for the development of analytical models.

1.1 Composite action structures

Historically, when steel frames began to be used to support cast-in-place RC slabs, the assumption was that the concrete slab acted independently of the steel frame so that they were considered as two, un-bonded, beam-like elements each of which carried load in a manner uncoupled to the other; i.e. no consideration was given to the composite effect of the steel and concrete acting together. With the advent of quality steels it became convenient to connect the concrete slab to the beam by welding shear-connectors in such a manner that the interface between the two resulted in a so-called *composite beam-slab* section. Initially applied to bridge

beams in the 1930s, composite construction was subsequently taken up in buildings in the 1960s; nowadays this technique has become common in many structural applications.

The extent to which the composite action is developed depends on the provisions made to ensure that a single linear strain from the top of the concrete slab to the bottom of the steel section is developed. The transmission of the shear forces and the stress distribution on the steel beam, the weld that connects the shear connector to the flange of the steel beam, the material of the connector itself (until recently only made of steel), as well as the strength of the concrete determine, not only, the effective stiffness of the connection but its ultimate strength.

A typical shear stud connector for a composite beam is shown in Figure 1 taken from {6} where the load deflection curves are indicative of local non-liner behaviour. The shearing force P is entered through the base of the shear connector into the concrete layer. The resulting local forces are shown schematically and are indicative of the how the internal force balance is achieved and the regions where, most likely, stress concentrations may result in failure of the constituent elements. So, for example, Pw is introduced at a small angle on the weld that connects the shear connector and the flange of the steel beam, so that at the root of the shear connector, concrete crushing may occur. The force transferred directly to the shank of the connector, Pb, may cause plastic deformations in the shank as well as tensile forces in the shear connector itself. These forces oppose the tendency of the slab to separate vertically from the steel beam. The shear forces along the height of the connector produce horizontal forces Pz which vary along the height and so generate an effective moment at the top of the connector resulting in local compressive stresses in the concrete at the full height of the stud. Depending on the dimensioning and quality of materials used, failure of the connection can occur at one or more of these sites.

There are many forms of shear connectors used in practice, but they can be divided into two types: flexible and rigid, according to the distribution of the shear forces and the functional dependency between strength and deformation.

Rigid shear connectors work by converting the shear stress in the concrete into shear loads in the stud (or other connector). Bending stresses can be disregarded so that on one side of the connector the concrete is predominantly in tension and on the other it is in tension. The high stiffness of the connector implies that its total deformation is small, resulting in localized stress concentrations in the surrounding concrete. If the load is sufficiently high, failure of concrete in compression or in the stud weld may result (the latter being fragile in nature).

Flexible shear connectors resist shear forces by a combination of bending, tension or shearing at the root. If the connection is flexible enough it is possible to develop plastic hinges away from the root weld. Flexible shear connectors exhibit more ductile behaviour; but, being more flexible, they are not as efficient at maintaining optimum shear transfer at moderate loads; thus, in general, the effective composite stiffness of beam-slab systems using flexible connectors is inferior to those using rigid connectors. In the limit, slack can develop at the transfer surface leading to a discontinuous shear transfer and loss of stiffness.

The type of shear connection employed in the PUMACOM bridge does not conform to any of the standard forms currently used in practice. To start off with, the usual the T, or I-shaped, steel beam section has been replaced by a carbon fibre sandwich box-beam. Secondly the individual metallic shear connectors have been replaced with a highly orthotropic pultruded glass-reinforced I-beam running across the width of the main carbon fibre beam. This type of shear connector is not well documented in the literature, and, whereas design of standards for shear connectors are widely available, none exists for FRP-to-FRP composite beam action.

The scope of this document is to provide some preliminary experimental results showing how such connectors transfer shear loads between the PUMACOM reinforced concrete slab and the carbon fibre beam.

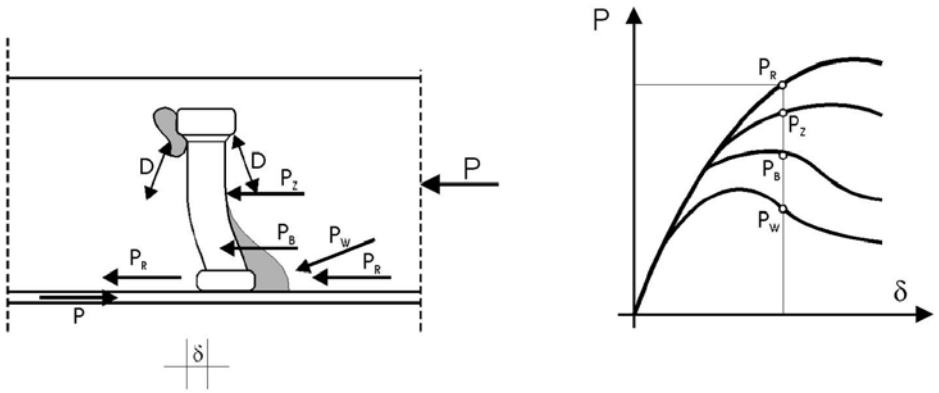

Figure 1 The shearing force distribution mechanism at a shear stud connector in a composite beam.

1.2Mechanical details of shear transfer system on PUMACOM bridge.

In a previous document {3} we have provided an extensive description of the design and manufacture of the carbon fibre composite bridge beam; however, for reference, at the end of this report we have reproduced some of the manufacturing and assembly details described therein. In Figure 3 we show the pultruded profiles as distributed onto the top of the carbon-fibre beam. The profiles were simply bonded using an epoxy adhesive, this thin bond layer provides the anchorage for the complete shear-lock mechanism. In between the main profiles, a second grid of smaller I-profiles layer is fitted. These profiles are longer and extent by 0.75m at either side of the carbon-fibre beam and provide the support used by the glass-fibre formwork that was used to pour the reinforced concrete for the bridge deck (see Figure 4). Both types of pultruded profile are manufactures from glass-reinforced vynelester resin. The dimensions of the profiles and their periodic distribution pitch is shown in Figure 5. The manufacturer quotes a flexural modulus of 20GPa in the plane of fibre reinforcement. The through-thickness modulus is not given, but given the modulus in this direction is resin-dominated it is expected that this cannot be more than 2-3 GPa..

Once the concrete has been poured a cross-section of the bridge beam and slab would appear as shown schematically in Figure 6 showing a generic shear loading between the concrete slab and carbon-fibre beam.

1.2.1 Some details on pultruded profiles

Pultruded profiles, like all composites, are characterized by highly orthotropic mechanical properties. They are composed of stratifications of glass-fibre embedded in a resin system that bonds the layers together. The layers are chosen in order to optimize the mechanical properties of the profile; a mixture of random fibre and cross-ply mats are placed alternatively; thus building up the required thickness. The layers are spliced one on top of each other to build up the thickness of the flanges and the web (this is shown schematically in Figure 2. Each layer in the laminate is configured so that the fibers are aligned in the direction of the local governing stresses, thus the tensile and compressive stresses in the profile are taken up primarily by unidirectional fibres in the direction of the main axis of the beam (strictly speaking the percentage of fibers is never 100% aligned in a single direction). The web usually contains a higher mixture of ±45º or other quasi-isotropic configuration in order to ensure sufficient shear strength and stiffness. The main structural weakness of pultruded profiles (or any FRP laminate) is the fact that, from a mechanical point of view, they are essentially two-dimensional objects; i.e. the through thickness properties are completely defined by the matrix and not the fibres.

1.2.2 Delamination of pultruded profiles

The web of a pultruded I-beam can be easily separated at either flange by applying a vertical tension force that causes delamination along the horizontal layers that make up the through thickness of the flange, much in the same way as it is easier to split wood parallel to the grain. Through-thickness stresses in laminates have been widely studied in the literature and are particularly harmful at fillet corners and joints {2{5}. Pull-out and bending stresses at the root of the I-beam shear connector used in the PUMACOM bridge can cause delamination stresses even if the predominant stresses in the main axis of the pultrusion (i.e. in the plane of the fibre alignment) are relatively low.

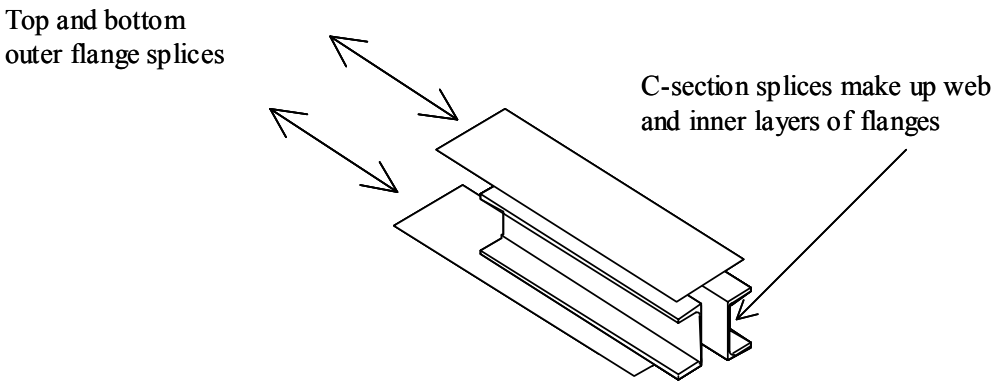

Figure 2 Generic lamination lay-up for pultruded beam.

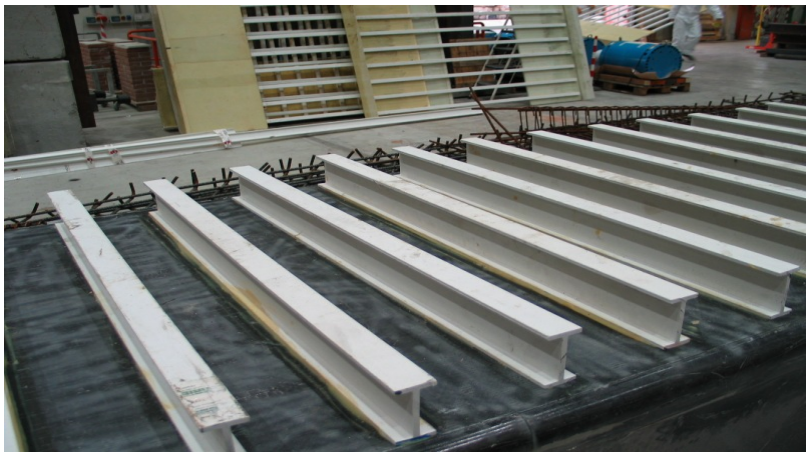

Figure 3 Pultruded shear-lock connectors bonded onto beam.

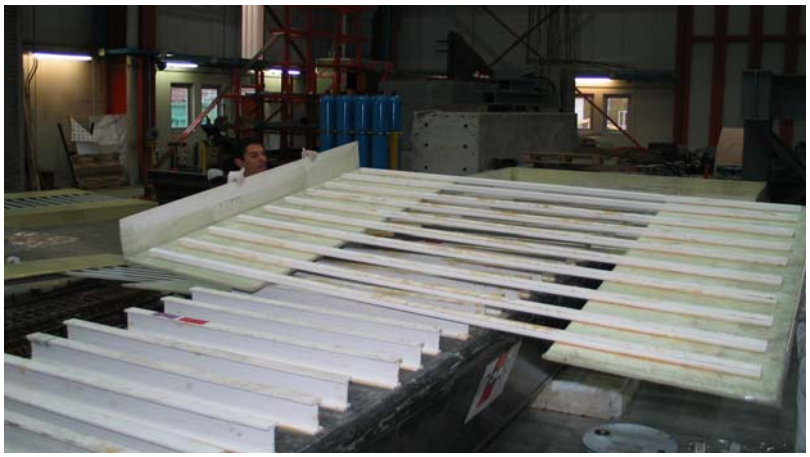

Figure 4 Detail of GFRP slab formwork slotted between the main shear-lock pultrusion beams

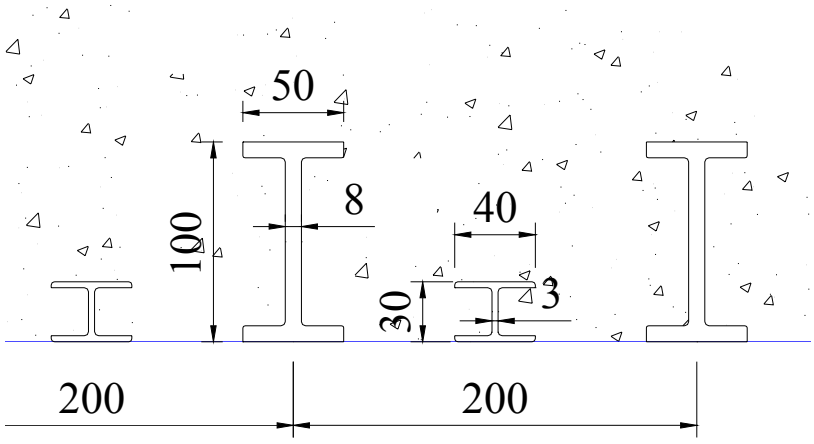

Figure 5 Dimensions (in mm) and pitch of shear connector pultrusions as mounted on carbon fibre beam.

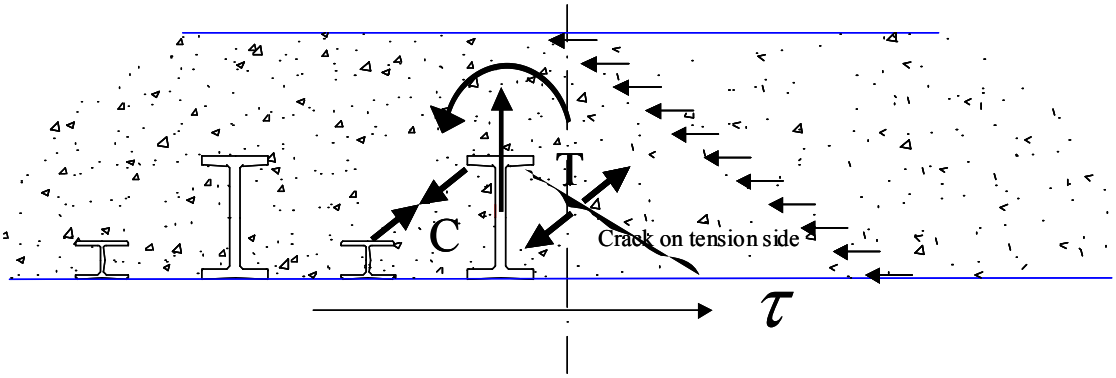

Figure 6 Generic shear force distribution along carbon-fibre beam and RC slab interface.

1.3 Instrumentation for monitoring shear interface

A full description of the complete instrumentation is given in {3}, however, in Figure 7 we show the positioning of the strain gauges embedded in the RC slab and interface which were situated at mid length of the main, 10 m span (note that the numbering is consistent with the plots given in this document). The position of the gauges along the beam length is such that it falls at half the distance between the rubber bearings through which the load is applied (see Figure 31) and run through the centre of the main beam axis. Along this interval of the beam the shear load is low but is subjected to high near-constant bending moment.

In order to monitor the efficiency of the beam composite action, we monitored the position of the neutral axis (NA) by placing strain gauges around the perimeter of the carbon fibre beam as shown in Figure 8. Finally a displacement sensor was bolted to the top-most layer of the concrete slab, from which it was possible to calculate the compressive strain in the top layer of the concrete slab. The calculated position of the N/A is measured from the interface between the concrete slab and the carbon beam: i.e. a negative value indicates that the NA is below the interface and hence within the carbon fibre beam.

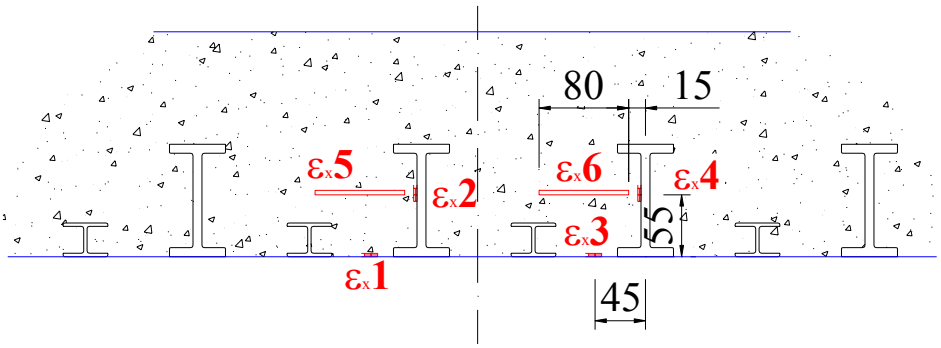

Figure 7 Position of embedded strain gauges (dimensions in mm).

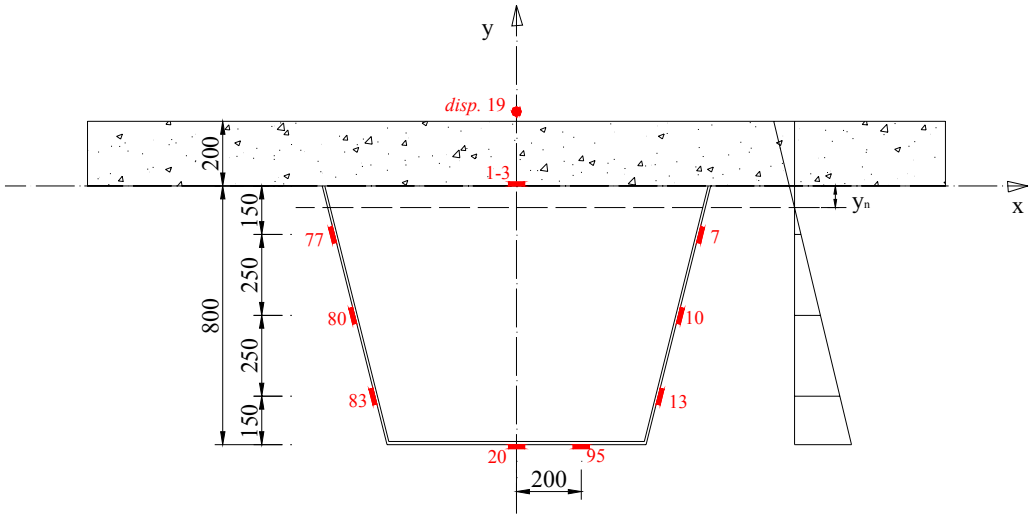

Figure 8 Detail of strain gauge positions used to evaluate the neutral axis at mid-span loading point. The NA is calculated by linear extrapolation of the weighted strains measured along the full height of the beam. The displacement channel mounted on the top-most layer of the concrete slab (No19) was also considered in the calculation.

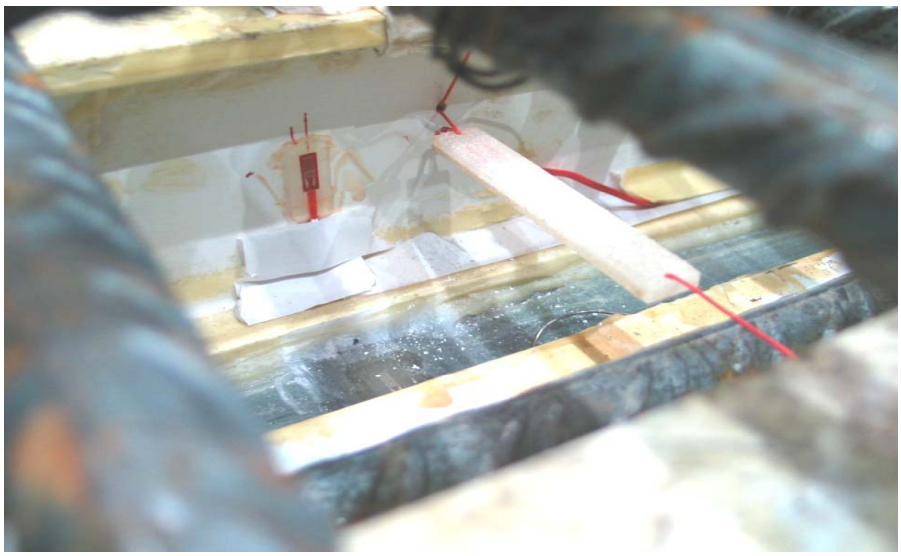

Figure 9 Detail of strain gauges to be embedded into concrete before pouring. The strain gauge mounted at mid height of the pultrusion's web can be seen clearly. The gauge is protected by a layer of low modulus polymer in order to avoid direct contact with the concrete grout. Slightly offset to the right, pointing towards the viewer, and laying parallel to the beam axis is the 'floating' RC strain gauge (also protected). The gauge mounted on the top-most layer of the carbon fibre beam is not visible.

.

2 Discussion of Results

The test campaign on the PUMACOM bridge assembly was described in detail in {3}. In this report we shall concentrate only on the performance of the shear connectors as measured by the strain gauges embedded between the carbon beam and the RC slab, but first we provide some background data on the concrete properties.

2.1 Compression tests on concrete coupons

The evolution of the concrete strength as measured from compressive tests on standard 150x150 mm coupons, is shown in Table 1and Figure 10. The specimens were cured under laboratory conditions similar to that of the concrete slab. The test campaign corresponding to the low level and proof tests was conducted 5 weeks after concrete pouring, thus the concrete strength was in excess of 37 MPa. The final destructive test was conducted four months after pouring of the concrete for which some marginal increase in concrete strength is to be expected.

Table 1 Concrete compression tests.

Date poured	*Test data*	*Days*	*Number of specimens.*	*Rck [MPa.]*	*fck [MPa.]*
14/11/2004	*19/11/2004*	*5*	*3*	*27.1*	*22.5*
14/11/2004	*26/11/2004*	*12*	*3*	*31.0*	*25.7*
14/11/2004	*03/12/2004*	*19*	*3*	*35.2*	*29.2*
14/11/2004	*16/12/2004*	*32*	*3*	*37.6*	*31.2*

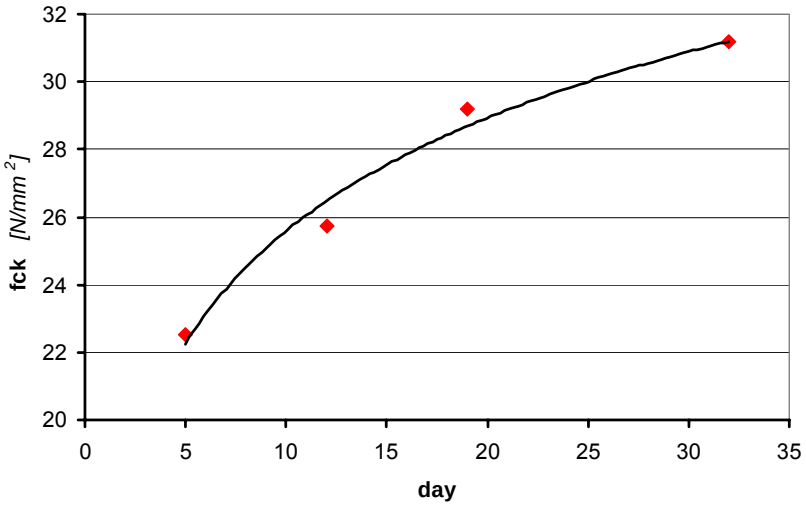

Figure 10 Evolution of concrete strength

2.2 Test T02

The loading protocol was scaled to reach 85 tons force i.e. 25 ton more than the proof load. The graphs of the single and total piston load; bending moment and shear force distributions are shown in Figure 11. The total force at the peak displacement is just over 86 tons with a corresponding maximum bending moment of 1.72MNm. The effective loads and the percentage loading at the supports A, B, and C (see Figure 33 and Figure 34 for details) are given in Table 2. The table gives the load at each support at the moment of peak total load. The percentage numbers give the proportion of the load taken up by each support. The near constant bending moment section between 4 and 6 metres from A is obtained by pairing the four piston forces into two piston pairs (the pair closest to A, at 4.3 metres, and the closest pair to B, at 5.7 metres). The moment between these points is not constant as it was found that the total load of the two pistons closest to A was slightly larger than those to the right of centre. Asymmetries in the structure mean that when the pistons come into contact with the beam deck, the local contact forces are slightly different from one piston to the next: this is inherent to the specimen and not the control strategy.

In Figure 12 we show the total piston force and centre-span moment versus central displacements, strains and curvatures. The maximum beam displacement at mid-span was just 21mm at 86 tons peak load. The force-displacement curves are hysteretic, but the permanent displacement when unloaded of less than 1 mm. The hysteresis is associated with initial cracking of the concrete deck at support B. However the width of the loop in terms of displacement is larger than that observed in terms of strain at mid-span. This is most probably due to the fact that spurious displacements of the supports further increase the displacement measurement at mid-span. In fact, the residual strain measurement upon unloading is of the order of 20με. In terms of moment curvature and moment strain the hysteretic curve is not as wide.

2.2.1 Strain measurements at the concrete carbon interface.

The data from the embedded strain gauges at mid-span are shown in Figure 13. The strain gauges mounted on the web of the shear connector pultrusions (ε_x2 and ε_x4) follow the general trend of the loading path; whereby tensile loading on the bottom face of the main carbon beam corresponds to a tensile strain in the web of the pultruded connector. Conversely, the strain in the gauges embedded in the concrete (ε_x5 and ε_x6) is compressive. The gauges mounted on the interface of the carbon fibre beam at the interface with the concrete are nearly zero indicating that these are situated close to the neutral axis. As we shall show below, this measurement does not correspond exactly with the estimation for the position of the NA obtained from the ring of strain gauges around the bridge-beam perimeter (to be explained below).

The strain readings of the gauges embedded in the concrete are in compression at peak load. On the basis of the strain readings, and assuming a Young's modulus for concrete of the order

of 25GPa, we estimate that the stress in the concrete is of the order of only 3MPa, and hence well below the ultimate strengths given in Table 1.

Given that in the central section of the beam loading train (between the two sets of steel-rubber bearings) the shear force is low and the moment is maximum and nearly constant, it is presumed that the tensile strains measured in the web of the shear-transfer pultrusions I-sections are due primarily to a tensile force rather than a local bending moment resulting from shear lag along the depth of the RC slab. If this were so, it would imply that the I-beam is being pulled away from its attachment on the carbon beam; thus the composite action (in the sense of classical composite beam-slabs) from the carbon-fibre beam to the concrete slab is through the adhesive bond between the lower pultrusion flange and the last layer in the carbon fibre beam. The state of stress in the concrete, being compressive, would indicate that the overall composite beam mechanism is one whereby the reinforced concrete slab in compression takes up the compressive flexural loads from the carbon-fibre beam. Thus the pultruded I-beams that act as connecting elements are subjected to pullout. As we mentioned above, the root of the connection between the pultrusion web and the flange is the weakest point as its properties are matrix-dominated and subject to delamination. In the event that failure should not occur in the pultrusion web-flange root, a similar type of failure (i.e. debonding) could occur at the interface between the pultrusions lower flange and the top face of the carbon fibre beam as, here too, the mechanical properties are solely defined by the bonding agent.

2.2.2 Neutral axis

The position of the neutral axis was calculated using the perimeter strain gauges mounted at mid span on the carbon fibre beam as well as the strain obtained from displacement transducer connected to the top surface of the RC deck as shown in Figure 8. The results are shown in Figure 14 where we have plotted the NA versus the central displacement (nominated as displacement data channel 4 in graph) at mid-span. The plot shows the loading and unloading paths. For very low displacement measurements the extrapolation of the NA is rather noisy and inaccurate, hence we can only consider the curve as valid in the range of 10-20 mm. We note that the curve is hysteretic and that the approximate location of the NA at peak load is about 20 mm below the interface between the carbon-fibre beam and the RC deck. This values is close enough (but still significantly different) to the actual position of the interface, where the strain gauges mounted at the top of the e carbon-fibre beam are close to zero, and hence would otherwise, define the position of the NA by definition as that section along the beam height where the strain is null. This small anomaly may be explained by the fact that whereas the overall neutral axis is in fact below the concrete-carbon beam interface, the flexibility of the shear connectors may result in localised load transfer redistribution at the interface: i.e. the shear distribution along the complete height of the bridge beam is locally not linear.

2.3 Test T03

In this test the generic loading-unloading path described in T02 was repeated with the target displacement extrapolated in order to reach 100 tons.

The graphs of the individual and total piston load, moment and shear force distributions are The shown in Figure 15. The total force at the peak displacement is just under 105 tons (see Table 2). The load distribution along the beam is comparable to that of T02, albeit at a higher load. As can be seen in Table 2 the load percentages taken up by the supports are also comparable to those of T02. The peak negative bending moment is of the order of 0.5MNm whereas the bending moment at the joint area is of the order of 1.0MNm. As expected the shear force is nearly zero in the interval of the piston loading train and changes sign at support B.

In Figure 16 we show the total piston force and centre-span moment versus central displacements, strains and curvatures. The force versus displacement plot shows that even for a load in excess of 100 ton the residual deformation upon unloading is less tan 1 mm. A comparable result is obtained for the moment versus centre-span curvature where the permanent residual curvature is less than 1/25 of the peak curvature.

The data obtained from the embedded strain gauges follows a similar pattern to that of T02, however the ratio of the tensile strains in the web between the central and the next-to-central pultrusions (see Figure 17) has been reduced compared to that of T02. The most notable difference is that whereas for T02 the pultrusion strain was completely recovered, in T03 we note that this is not the case; however, it is not clear whether this effect is due to local damage of the pultrusion or as a result of the local crushing of the beam at support B. The ratio of the strains measured within the concrete seems to be unaltered, whereas the strains on the surface of the carbon fibre beam, although still rather small, are of differing sign. In Figure 19 we compare the hysteretic cycles of T02 and T03 from where we note that, although in terms of force-displacement and force-strain, there does not seem to be any apparent degradation, the curvature plots indicate that some loss of stiffness has occurred. However, the position of the neutral axis at peak load (Figure 18) appears to have been raised (now only 15mm below the interface). We cannot account for this discrepancy unless we assume a discontinuity has arisen at the beam-slab interface.

2.4 T05: Test to failure

From the total force-displacement and moment-central strain plots, shown in Figure 20, we follow the overall performance of the bridge deck up to failure. The bridge beam failed at just less than 134 tons as a result of the failure of the joint connecting the two main carbon fibre beam elements that make up the 13m beam length (which was discussed at length in {3}), however the fragile failure of this joint was first preceded by a non-linear softening resulting from the crushing of the beam support at B.

The results of the calculated forces are shown in Figure 21. The unbalanced vertical equilibrium force measurement error compiled from the individual support reaction forces is acceptably low (not exceeding 5tons). It can be seen that the loads measured at C and B drop off

considerably when the total force signal enters the non-linear regime. In the same figure we show the calculated moment and shear force diagrams.

Returning to the force-displacement data in Figure 20, we note that for loads in excess of 110 tons (>25 mm central displacement) the force-displacement curve exhibits non-linear, softening, behaviour. From Table 2 we can see that the load percentages taken up by the supports have altered considerably compared to T02 and T03. At point 720 the percentage taken by support B has gone up to 84% of the nominal central load, however at peak load the percentage taken by support C is only 15 %.

2.4.1 Strains analysis

The strains in the pultrusion (ε_x2 and ε_x4) show a marked qualitative difference with respect to T02 and T03, for it can be seen that upon loading the strains are initially compressive (see Figure 22). This will have implications concerning the starting position of the NA. Moreover, the peak strains do not coincide with the point at which the main beam failed (partial strain relaxation precedes ultimate failure). We conjecture that this is due to the fact that the loading configuration of the bridge deck was considerably affected by the crushing of the support at B.

Whereas the concrete strains (ε_x5 and ε_x6) remain compressive, the strains in the carbon fibre interface show a marked negative trend implying that the position of the neutral axis has shifted noticeably below the slab-beam interface. In fact in Figure 23 we note that the position of the NA —as calculated from the perimetral strain gauges—has been lowered considerably. Starting from a position below that obtained from the previous test, the NA drops quickly upon loading to approximately 70 mm under the interface ,at a beam deflection of 15mm. However, this does not occur at peak load. In fact, the NA at peak load is approximately 50 mm below the slab-beam interface and remains there until the structure fails catastrophically. We cannot account for this behaviour other than to note that, indeed, as we noted earlier, the strain distributions at the slab interface were noticeably different from those of previous tests. It is possible that although the final failure eventually occurred at the wet lay up joint where the two main carbon-fibre beam sections are connected at 2.5 m from support B, the shear transfer capacity between the slab and the carbon beam had degraded to a point where some of the composite beam stiffness capacity had already been lost as manifest by the absolute negative values of the strain gauges mounted on the carbon-fibre beam at the RC interface (ε_x1 and ε_x3)

Table 2 Peak forces and moments.

		$Force^{max}$ [KN.]	R_A [KN.]	R_B [KN.]	R_C [KN.]	M^{max} [MNm.]	M^{min} [MNm.]
T02		862 *(100%)*	419 *(48%)*	661*(76%)*	198 *(23%)*	1.72	-0.42
T03		1042 *(100%)*	480 *(46%)*	806 *(77%)*	245 *(23%)*	2.00	-0.57
T05	*Point 720*	1042 *(100%)*	413 *(40%)*	875 *(84%)*	292 *(28%)*	1.81	-0.80
	peak	1334 *(100%)*	595 *(45%)*	914 *(68%)*	201 *(15%)*	2.60	-0.55

3 Conclusions

We have analysed the performance of pultruded shear connectors mounted on a composite-action carbon fibre bridge beam by monitoring the strain distribution at the RC slab-beam interface.

We have found that the capacity of the shear connectors to generate the composite beam action is highly effective up to a factor of 1.75 times the proof load. The measured position of neutral axis of the bridge beam is close to the desired position; corresponding to the interface line between the slab and the carbon fibre beam. The strain levels in the web of the pultruded shear connectors was an order of magnitude below the expected failure strain of the material in the plane of the reinforcing fibres and is representative of flexible, rather than rigid shear connector, however, even these low strain levels could promote the formation of delamination resulting from pull-out of the web-flange root at the point where it is bonded to the top surface of the main carbon-fibre beam. Although the pultruded shear connector is locally much more flexible that the more usual rigid steel studs, the fact that the pultrusion acts along the whole width of the carbon beam ensures a good overall shear lock resulting in a highly effective shear lock system.

At higher loads, and leading up to failure of the bridge beam itself at 134 tons, it was found that although the shear connectors did not fail before the carbon fibre beam itself, the distribution of the strains on the connector was qualitatively different from that observed at lower load levels. This could be indicative of incipient delamination of the web-flange root or the bond line between the pultrusion and the carbon fibre beam itself. In view of the potential weakness in this area, it is possible that fatigue loading could provide a mechanism for delamination at lower loads. It is expected that extended monitoring of the real installed bridge will provide further experimental data on the degradation of the interface due to environmental and fatigue loading.

References

{1} M. Bruneau and D. Walker, "Cyclic testing of pultruded fiber-reinforced plastic beam- column rigid connection", Journal of structural eng. ASCE, vol 120, N0 9, Sep. 1994, 2637-2652.

{2} A. J. Bass and J. T. Mottram, "The behaviour of connection in frames of fibre-reinforced polymer sections", Structural Engineer, 72/ **17 (1994), 280-285**

{3} E. Gutierrez, S. Primi, P. Caperan et al, "PuMaCom Project", Technical Note No. I.o4.74, ELSA-IPSC-JRC, European Commission, May 2004.

{4} E. Gutierrez, G. Verzeletti, C. Galiotis, "Application of composites to civil engineering structures; shear and bending of beam-to-column composite sections:,Advanced Composite Letters, Vol. 6, No 2, 1997, 47-52.

{5} A. S. Mosallam, M. K. Abdul-Hamid and J. M. Conway, "Performance of Pultruded FRP connections under static and dynamic loads", Journal of Reinforced Plastics and Composites, 13 **(1994), 386-407**

{6} S. Ranković, D. Drenić, "Static strength of the shear connectors in steel-concrete composite beams: regulations and research analysis", Facta Universitatis Series: Architecture and Civil Engineering Vol. 2, No 4, 2002, 251 - 259

Acknowledgements

The authors would like to acknowledge the commitment of NECSO (Nueva Entrecanales y Cubiertas) that for the funding and development of the PUMACOM project. The experimental results served as the basis for the study reported herein.

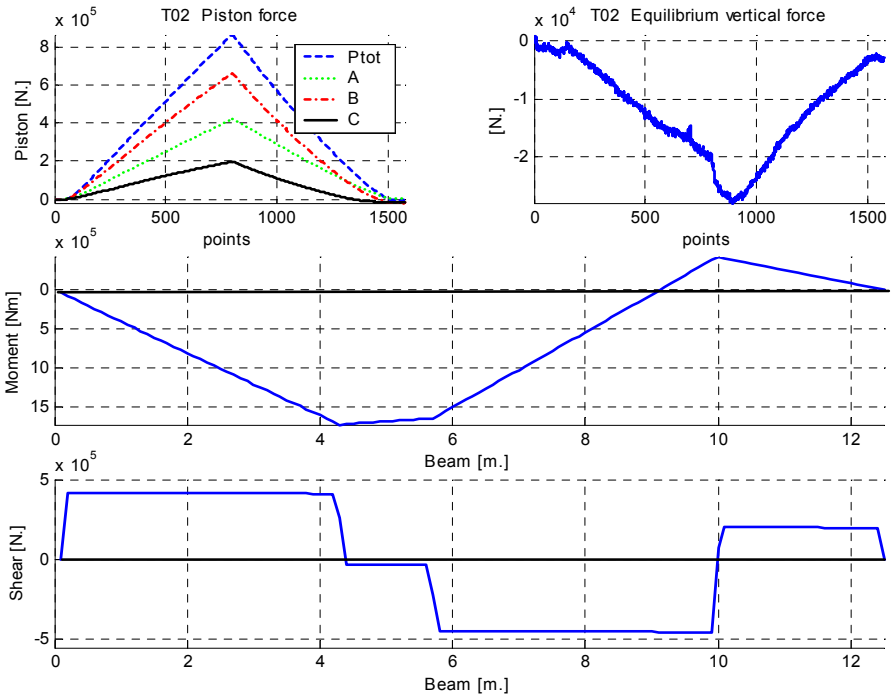

Figure 11 T02: Forces, moment and shear force diagrams.

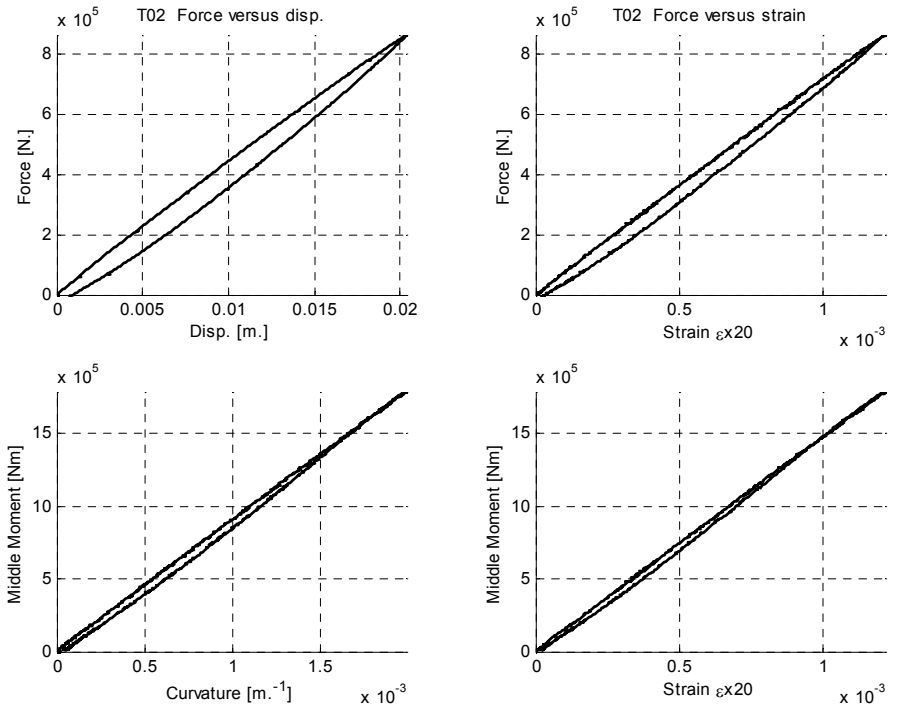

Figure 12 T02: Hysteresis cycles.

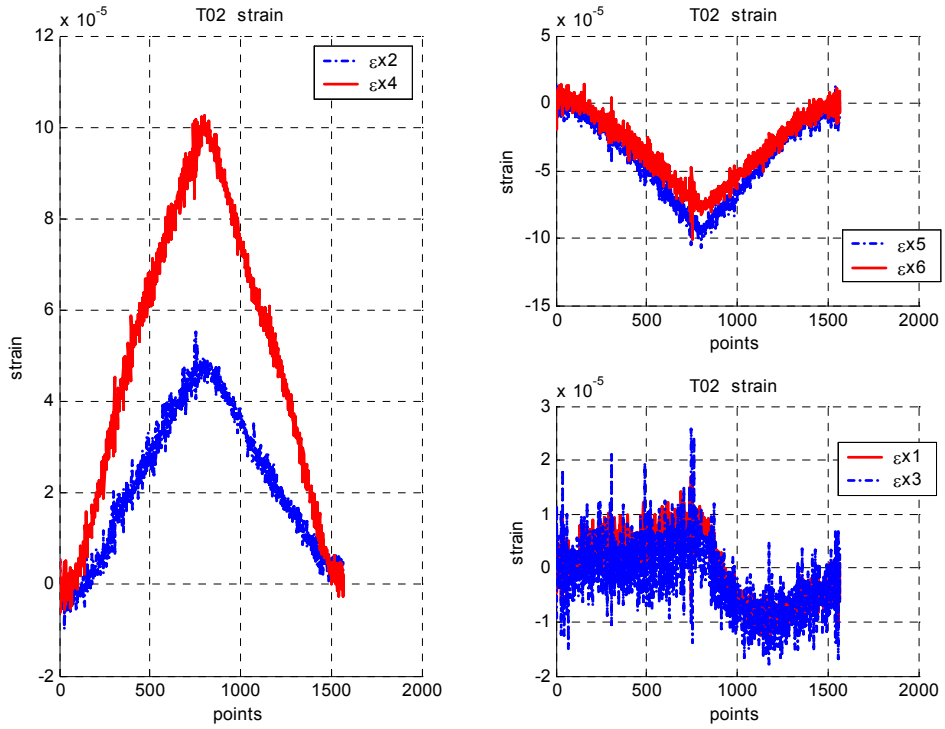

Figure 13 T02: Embedded strain gauges.

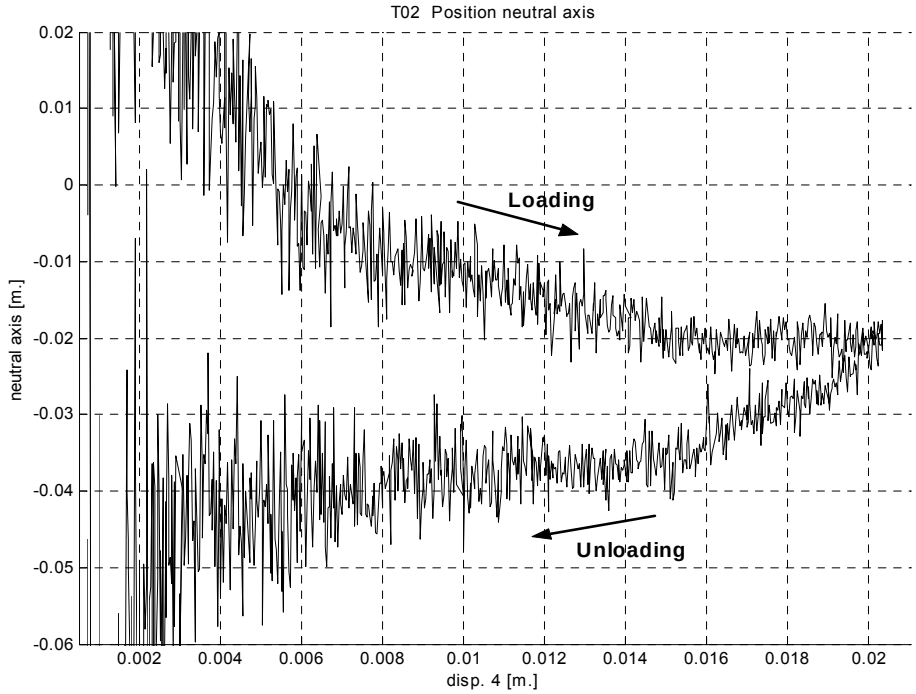

Figure 14 T02: Position of neutral axis.

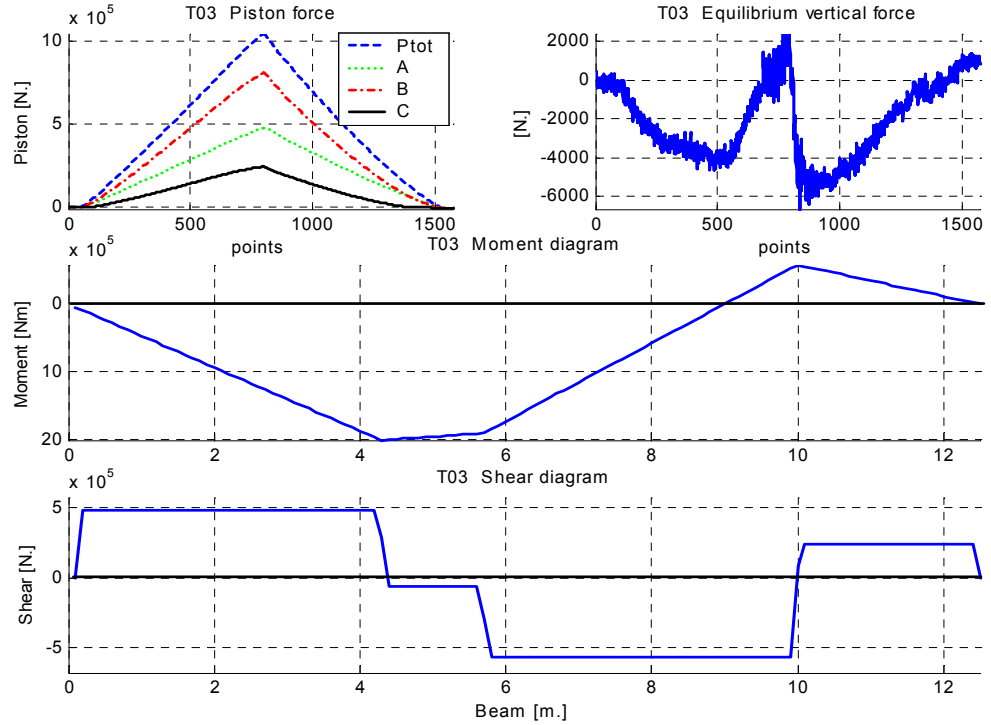

Figure 15 T03: Forces, moment and shear force diagrams.

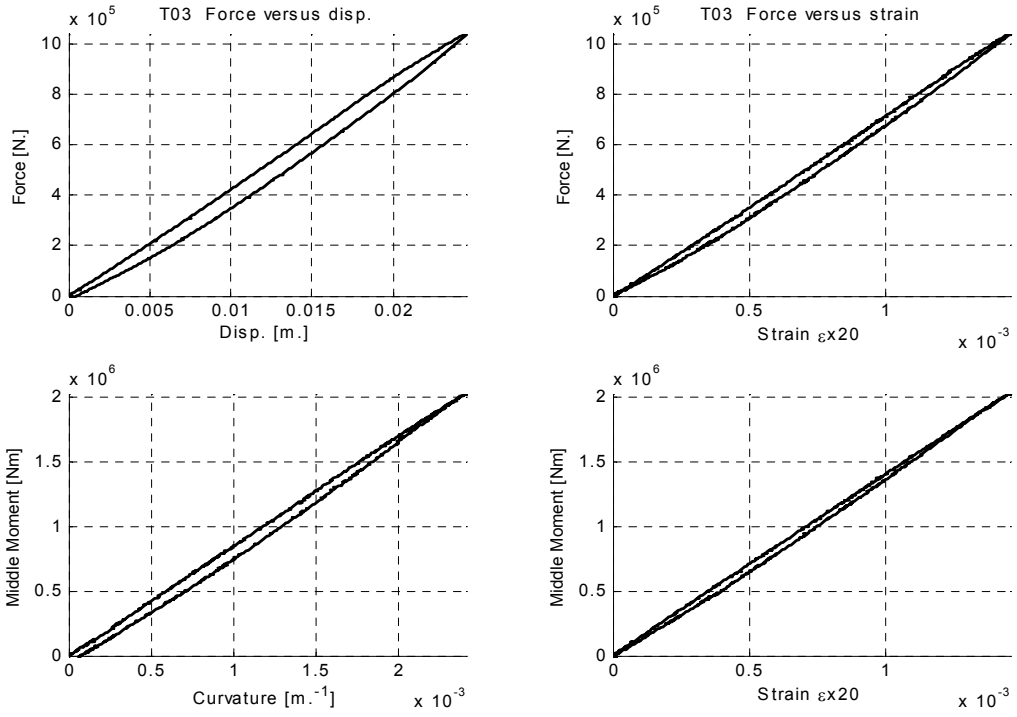

Figure 16 T03: Hysteresis cycles.

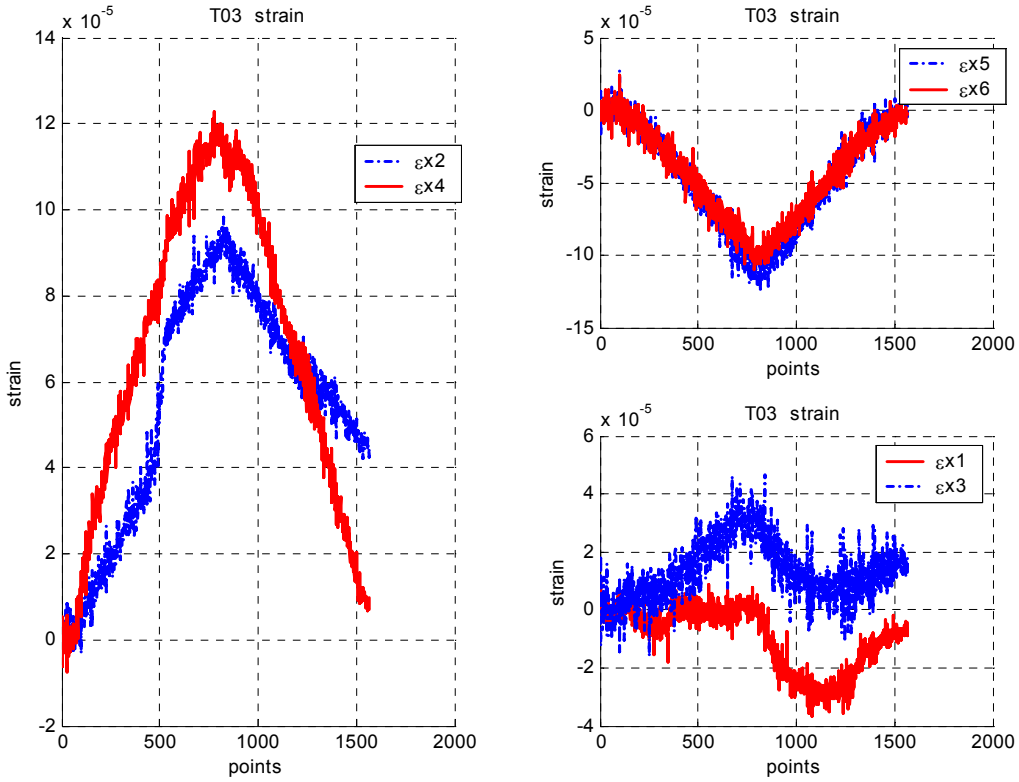

Figure 17 T03: Embedded strain gauges.

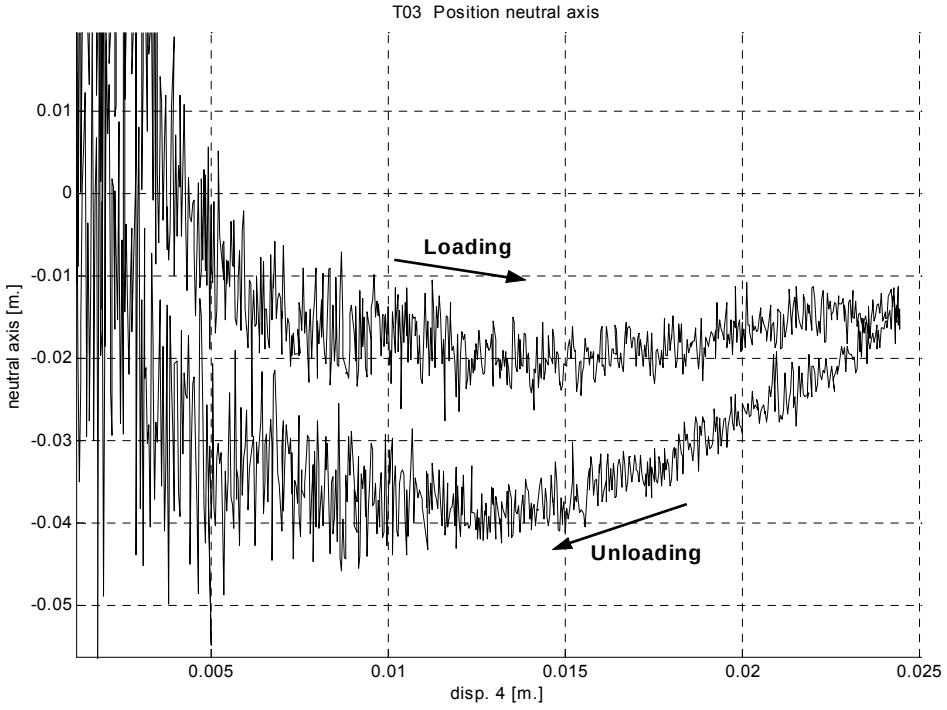

Figure 18 T03: Position of neutral axis.

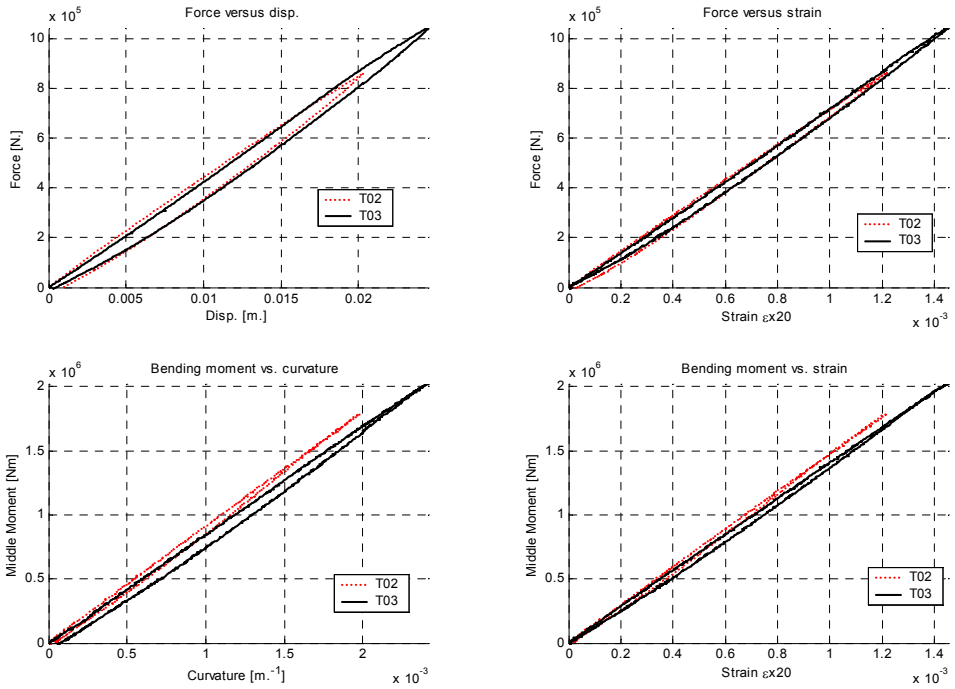

Figure 19 Hysteresis cycles T03 and T02.

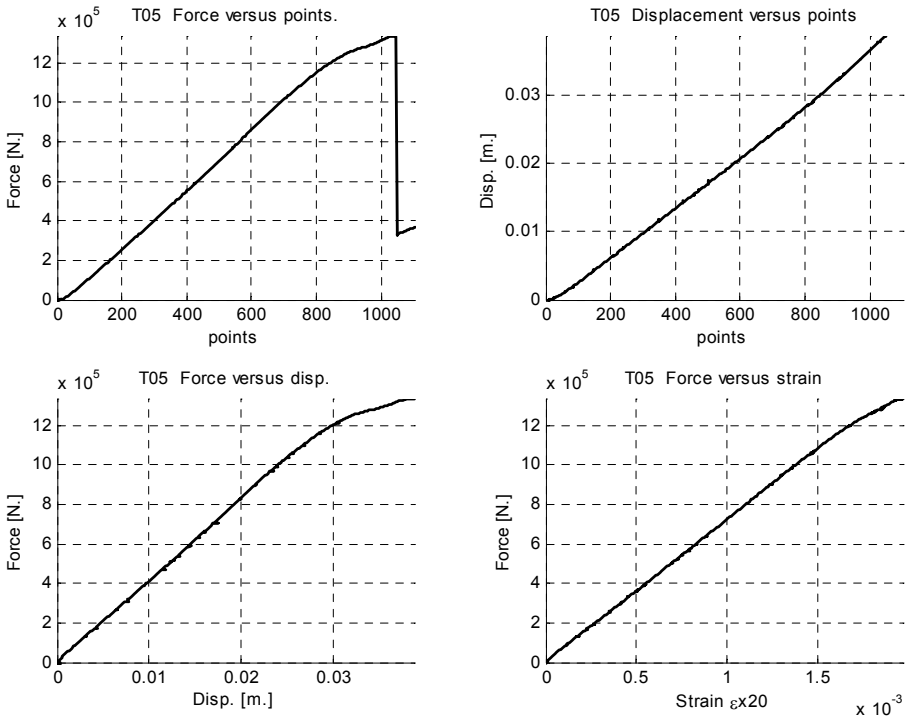

Figure 20 T05: Force versus displacement and strain at mid span.

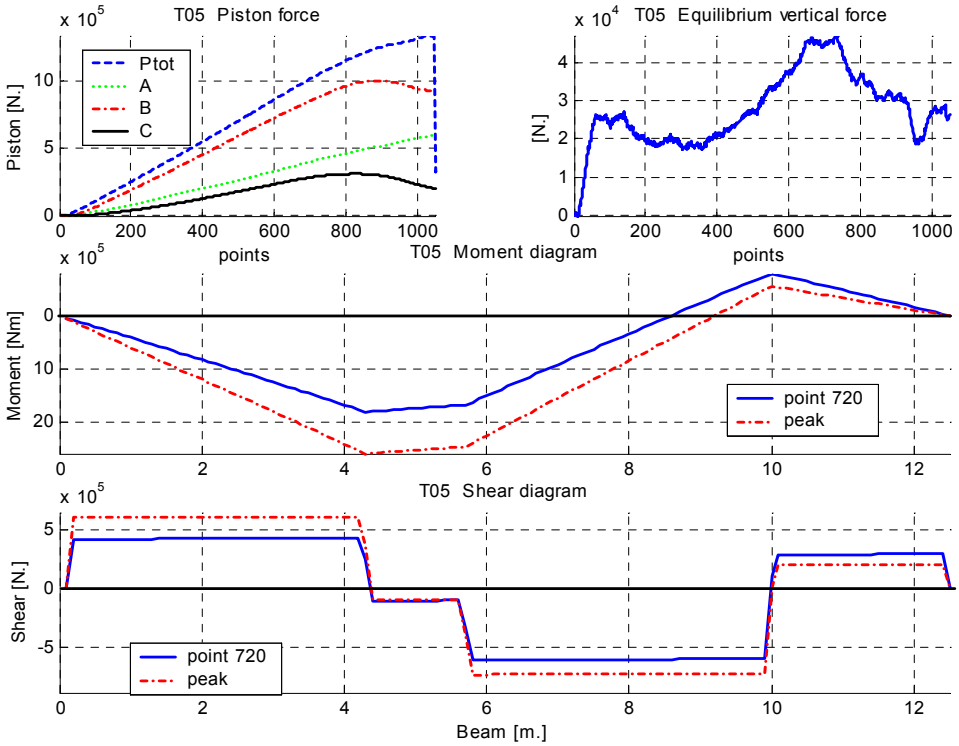

Figure 21 T05: Forces, moment and shear force diagrams

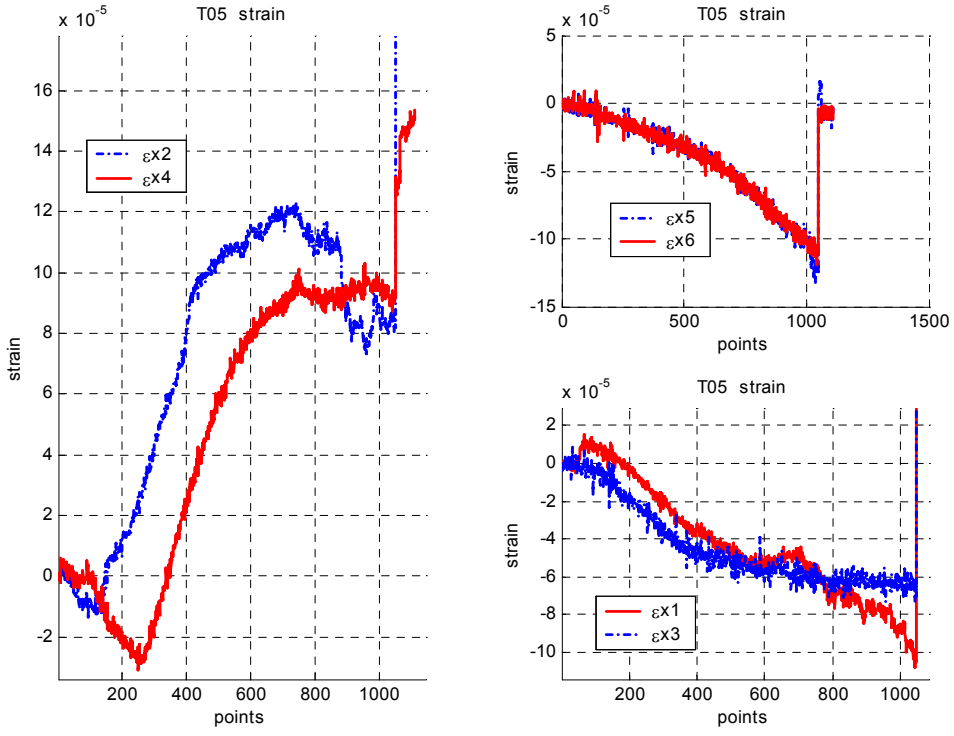

Figure 22 T05: Embedded strain gauges.

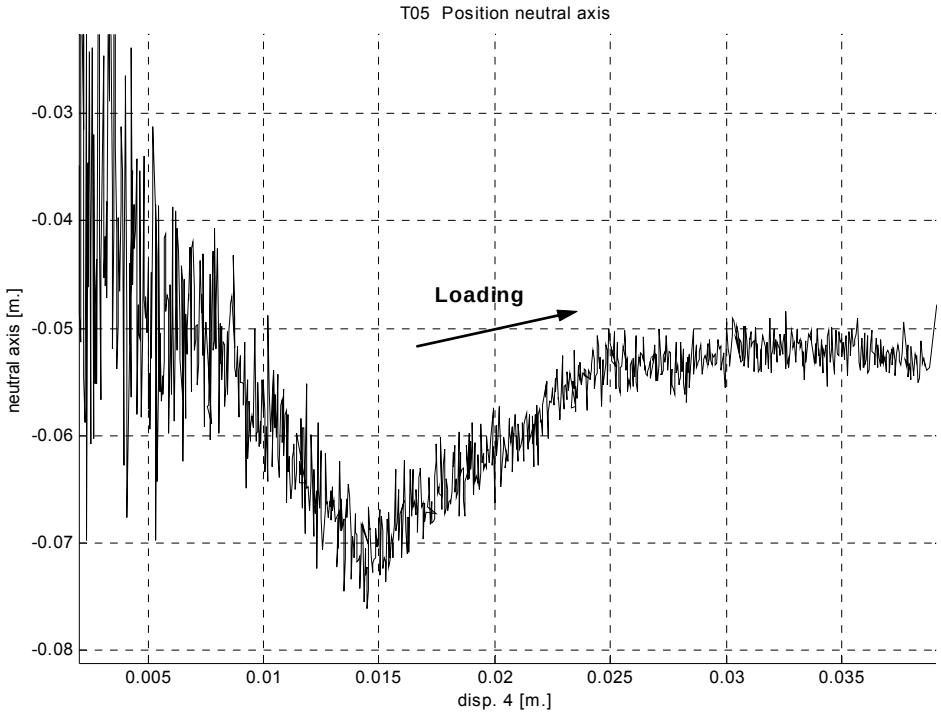

Figure 23 T05: Position of neutral axis.

4 Generic details of the bridge

The bridge design consists of a 46-metre long hybrid carbon-fibre beam connected to a reinforced concrete deck. The structural concept is similar to standard composite action bridge-deck systems, except that a carbon fibre beam replaces the usual steel superstructure. One of the advantages of using carbon-fibre systems is that they can be manufactured off site and are light enough to be transported to the motorway location and assembled on site using less onerous lifting equipment. In fact, the other main structural component, i.e. the RC slab, was manufactured using lightweight, glass-reinforced lost-formwork systems that will not require scaffolding and other expensive logistics, such as heavy cranes or transport machinery. In Figure 24 and Figure 25 we show the plan and side views of the bridge

4.1 Beam design

The carbon fibre bridge beam is made up of two lengths (7.5 and 5.5 metres) joined about their matching perimeters with a 0.6 metre wide, wet lay-up, stitch-bonded carbon fibre splice. Sections through the beam are given in Figure 26 to Figure 28. It consists of medium density ($40kg/m^3$) polyurethane foam that provides the profile shape for the carbon-fibre beam itself. Layers of pre-impregnated (pre-preg) carbon fibre cloth are draped around and along the length of the foam core in order to provide both tensile and shear reinforcement. The carbon fibre material is bonded onto the foam by submitting it to a low temperature curing cycle at 80^o C for five hours. The bonding process is aided by applying a vacuum around the beam that compresses the carbon fibre layers directly onto the foam mould. Because the bridge has stringent deflection serviceability requirements, the carbon-fibre laminate must be capable of withstanding large temperature excursions without loss of stiffness, hence even though the manufacturing process must be conducted at low curing temperatures, the glass transition temperature (Tg) of the material must be higher than 100^oC. For this reason the low temperature curing resin system VTM26 produced by the Advanced Composites Group was used, which can provide the laminate with a Tg of up to 120^o when cured at 60^o C for 10 hours.

The main structural element is composed of a carbon-fibre sandwich beam with a linear weight of approximately 90kg per metre length. The lay up of the carbon fibre laminate is shown schematically in Figure 26 and the resultant laminate properties for the various sections are given in Table 3.

The distribution and orientation of the carbon fibres on the beam laminate (predominantly at 0^o on the top and bottom flange faces and 45^o on the web side panels) results in highly anisotropic properties. The bottom flange contains the highest percentage of unidirectional fibres in order to provide sufficient tensile capacity. The percentage is lower for the top flange as it is expected that the concrete slab will carry the compression load. Combining these flexural layers with the bulk of the sandwich foam core ensures both a high tensile stiffness and a high buckling load capacity on the web panels, for which the thickness of carbon fibre skin would, by itself, not be enough to provide adequate stability. Thus, although the web has a low tensile modulus, that in shear is high, resulting from the fact that it is made up mostly of unidirectional fibres at $\pm 45^o$ to

the main beam axis. Consequently, the web Poisson ratio is 0.77, which for an isotropic material is physically inadmissible, but for composite materials is quite typical.

On the top surface (i.e. in contact with the concrete), rows of glass-fibre reinforced polymer (GFRP) pultrusions are periodically placed –crosswise– to act as shear connectors between the carbon-fibre beam and the concrete decking. These critical elements perform the same mechanical function as shear-stud connectors in classical composite beams, which generate the stiff monolithic composite action. The concrete slab is poured into a GFRP lost-formwork bonded onto the top layer of the carbon-fibre beam surface. The dimensions of the RC bridge deck are 2.7 metres wide and 0.2 m thick and reinforced with steel bars (subsequent designs will substitute these with GFRP re-bars).

Table 3 Mechanical properties.

Mechanical properties	*Top flange*	*Bottom flange*	*Web*
E_1 *[MPa.]*	77.125	98.000	14.000
E_2 *[MPa.]*	17.300	9.833	14.000
E_3 *[MPa.]*	4.000	4.000	4.000
G_{12} *[MPa.]*	13.500	8.330	29.500
υ_{12}	0.63	0.5	0.77
υ_{21}	0.13	0.06	0.77
F_1 *[MPa.]*	938	1083	500
F_2 *[MPa.]*	245	111	500
F_{12} *[MPa.]*	300	167	700
α_1 *(10^{-6} ºC)*	0.6	0.4	5

4.1.1 Assembly and Construction at ELSA

The carbon-fibre sandwich beam can be seen in Figure 29 being manoeuvred into position prior to the placement of the GFRP slab formwork. The pultruded shear-lock connectors are shown in Figure 3 ,in Figure 4 we show how the slab formwork was put into place, and in Figure 30 the deck fitted with the reinforcing steel. The beam was mounted between two RC blocks in order to simulate the supports piers in the real bridge. During the pour no props were used to support the carbon fibre beam as it is designed to be stiff enough to carry the 17 tons weight of the poured concrete with only a 4 mm deflection. This highlights the advantage of using lightweight composites as self-sustaining formworks. However, restraints were used at either end of the deck in order to prevent rocking and overturning of the beam about its main axis. Such constrains was not required when the full bridge was assembled in the real work-site because the ends were prevented from twisting by the combined constraint generated by mounting the three beams side by side. Moreover, the ends were built in at the bridge abutments thus further preventing unwarranted displacements during pouring. Supports were provided in order to avoid permanent deformations in the overhangs of the RC deck, but the carbon fibre beam carried the main load at all times.

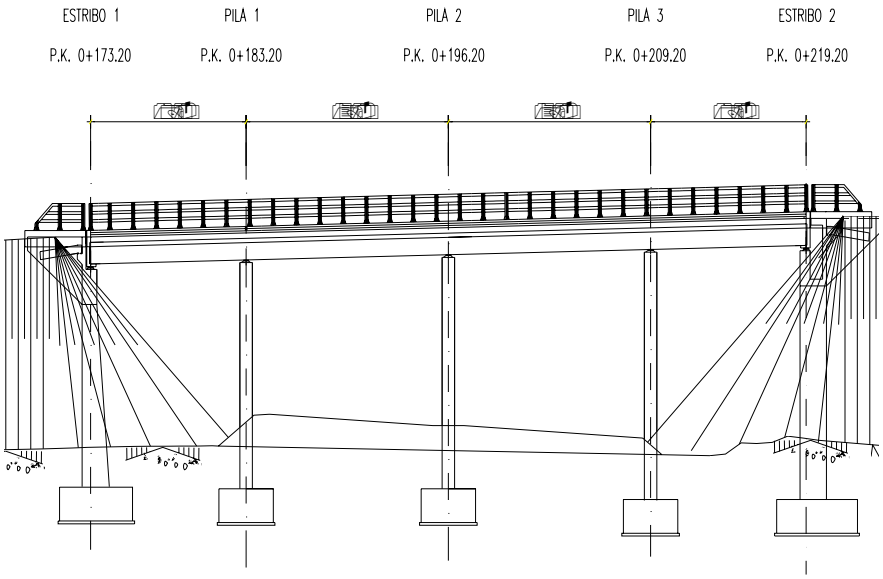

Figure 24 Longitudinal profile of the bridge.

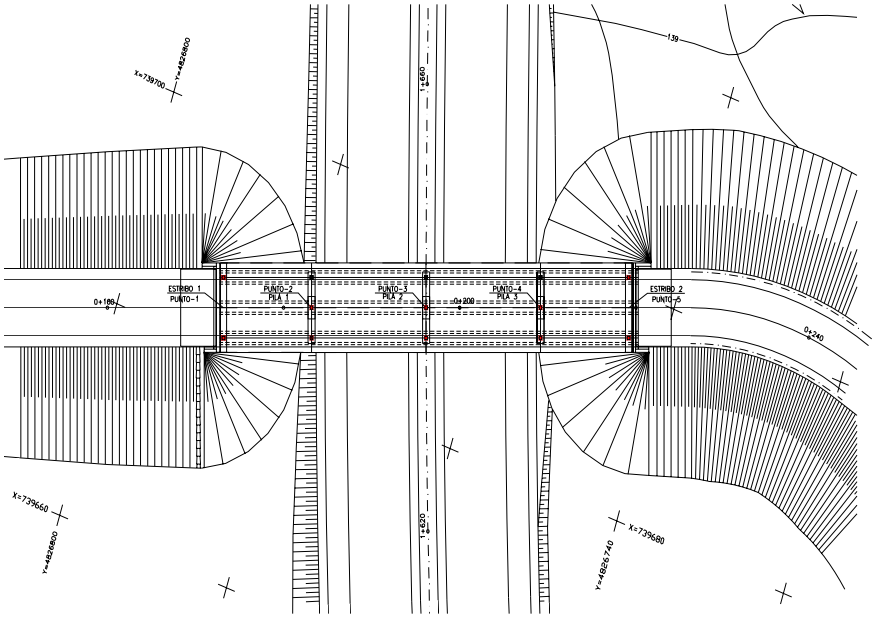

Figure 25 Roadway, alignment of the overpass.

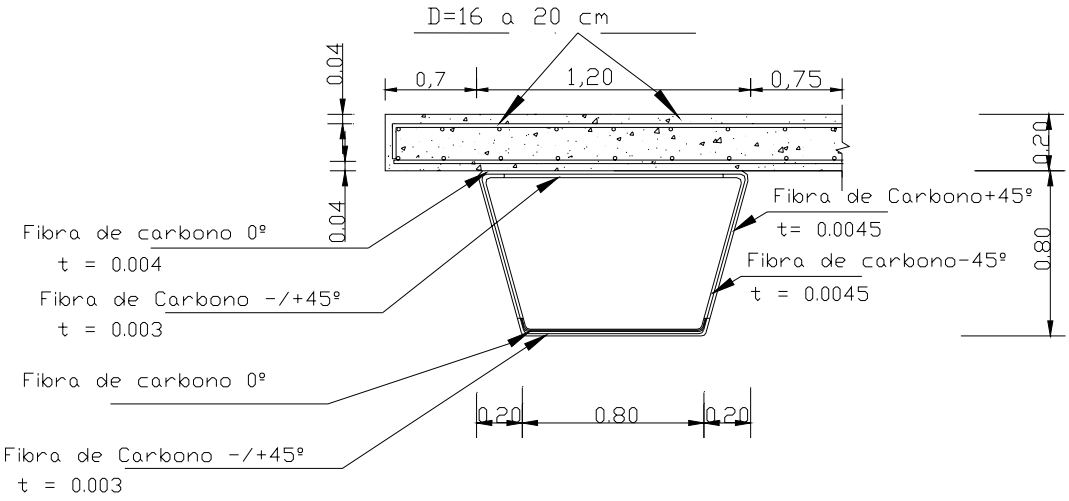

Figure 26 Cross section.

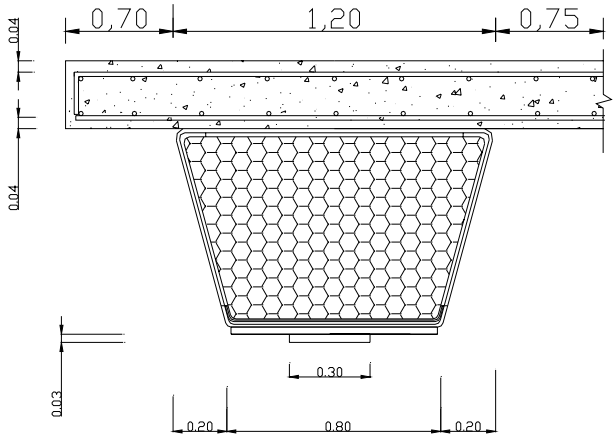

Figure 27 Cross section on support.

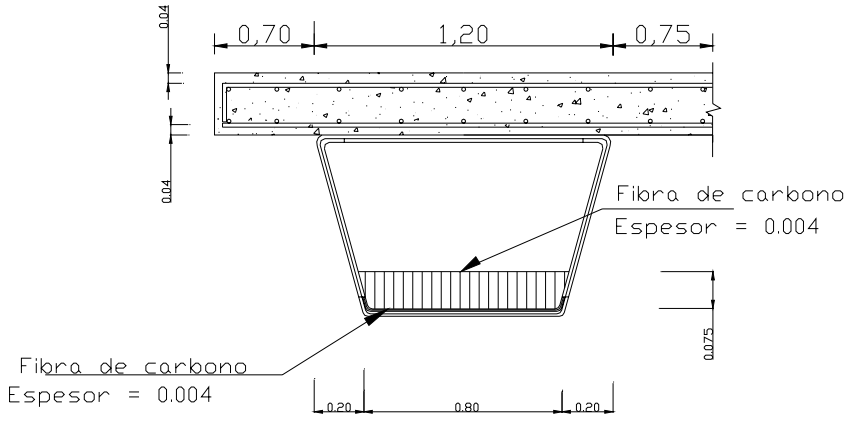

Figure 28 Cross section of support diaphragm area close to support.

Figure 29 Carbon fibre beam.

Figure 30 Reinforcement of RC deck.

4.2 Loading

The loading of the beam was performed under displacement control mode. The mechanical set-up for loading is shown in Figure 33 and Figure 34. Each piston is commanded individually from its own command computer. The loading protocol is the same for all controllers: it consists of simple saw-tooth loading and unloading ramps. All four pistons move at the same rate and apply the same nominal displacement to the centre of the bridge mid-span.

The main objective of the test campaign was to evaluate the stiffness of the bridge beam and compare it to the design calculations. The deflections of the structure under different loading combinations govern the serviceability limit design of the bridge; for these we performed low level and proof load tests. The designers also needed to know the ultimate capacity of the bridge; hence a test up to the ultimate failure load was also required.

Figure 31 View of loading train steel-rubber bearings.

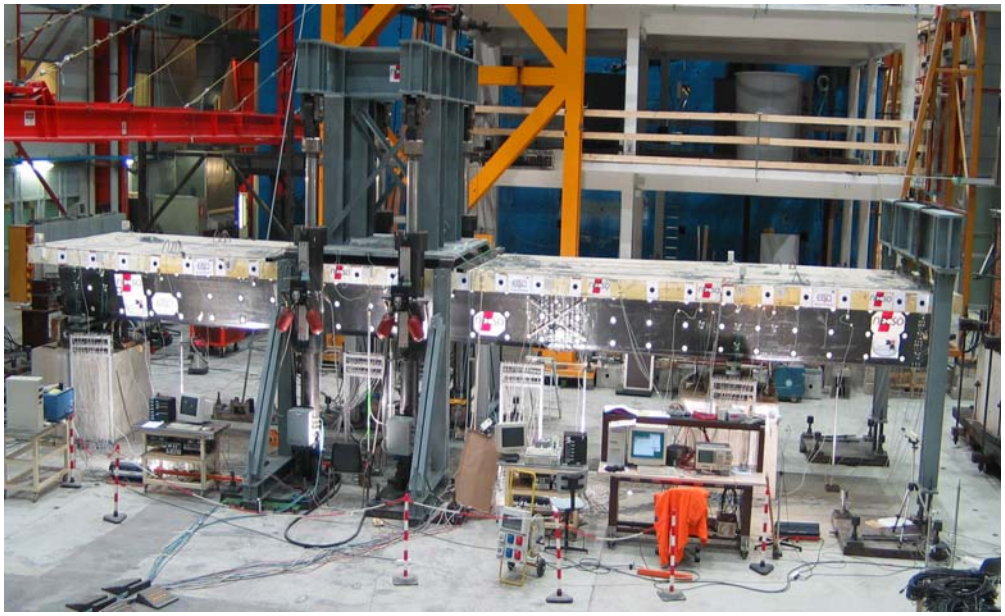

Figure 32 PUMACOM bridge with full instrumentation, ready for testing

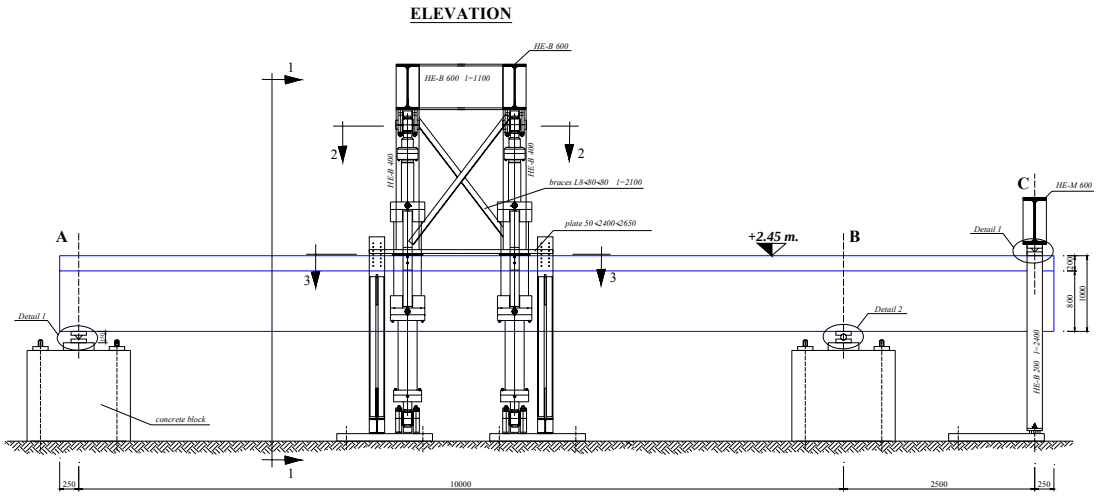

Figure 33 Loading rig set up, elevation.

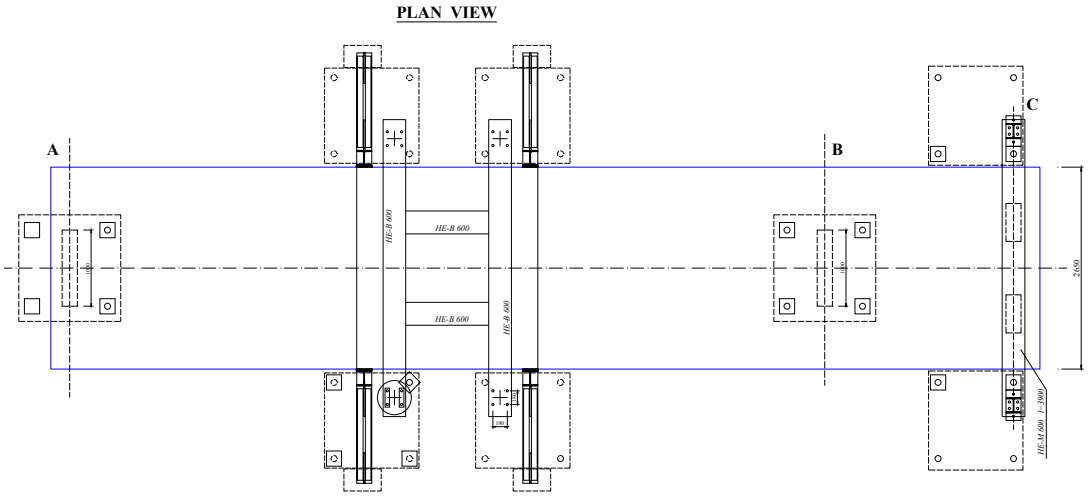

Figure 34 loading rig set up, plan view.